Supplementary Materials for Strength-ductility materials by engineering coherent interface at incoherent precipitates

Dongxin Mao,[1†] Yuming Xie,[1,2†] Xiangchen Meng,[1,2†] Xiaotian Ma,[2] Zeyu Zhang,[1] Xiuwen Sun,[1]

Long Wan,[1] Korzhyk Volodymyr,[3] Yongxian Huang[1,2]*

[1]State Key Laboratory of Advanced Welding and Joining, Harbin Institute of Technology, Harbin 150001, China

[2]Zhengzhou Research Institute, Harbin Institute of Technology, Zhengzhou 450000, China

[3]The E.O. Paton Electric Welding Institute of the NASU Kazymyr Malevich Str. 11, 03 150 Kyiv, Ukraine

[†]These authors contributed equally to this work.

*Corresponding authors. Tel.: 86-451-86413951. E-mail: yxhuang@hit.edu.cn (Yongxian Huang).

- **Table S1. Chemical composition of 2195 alloy (Discussed in "5.1 Materials and preparing process":1st paragraph)**

2195 powder	Cu	Li	Mg	Ag	Zr	Fe	Al
Mass percentage (wt.%)	3.99	1.09	0.38	0.42	0.1	0.17	Bal.
Atomic percentage (at.%)	1.68	4.19	0.43	0.10	0.03	0.08	Bal.

- **Table S2. Crystallographic information of the phases (Discussed in "2.2 Coherent-incoherent precipitates and fine grains":7th paragraph)**

Phase type	crystallographic information	plane	interplanar spacing(nm)	Angle between planes(°)
Al matrix		No.1:-1-1-1	2.3379	No.1/2:109.47
		No.2:-111	2.3379	No.2/3:54.74
		No.3:-200	2.0247	No.1/3:54.74
Al_7Cu_2Fe		No.1:202	2.9145	No.1/2:65.37
		No.2:21-4	2.2536	No.2/3:27.99
		No.3:41-2	1.50489	No.1/3:37.37
Al_2Cu		No.1:200	3.0327	No.1/2:45.00
		No.2:110	4.2889	No.2/3:26.57
		No.3:310	1.9180	No.1/3:18.43
Al_3Zr		No.1:114	2.3701	No.1/2:53.76
		No.2:200	2.0045	No.2/3:24.45
		No.3:314	1.2165	No.1/3:29.30

- **Table S3. The disregistries δ between different interfaces (Discussed in "3.1 Microstructural evolution":6th paragraph)**

Different interface	$[uvw]_{Al}$	$d_{[uvw]Al}$	$[uvw]_{Al2Cu}$	$d_{[uvw]Al2Cu}$	θ	δ_i	δ
	[]	2.225	[200]	2.887	19.18	27.21	
Al-Al_2Cu	[00]	1.963	[110]	4.140	10.20	53.33	34.5
	[11]	2.225	[020]	2.887	2.86	23.03	
Differed interface	$[uvw]_{Al}$	$d_{[uvw]Al}$	$[uvw]_{Al7C2Fe}$	$d_{[uvw]Al7Cu2Fe}$	θ	δ_i	δ
	[]	2.225	[0-16]	2.223	0.64	0.08	
Al-Al_7Cu_2Fe	[00]	1.963	[202]	2.946	12.66	34.99	15.7
	[11]	2.225	[21-4]	2.275	25.61	11.81	

- **Fig. S1-S2: The distribution of Al_2Cu/Al_7Cu_2Fe in commercial 2195 alloy and DDMed 2195 alloy (Discussed in "2.2 Coherent-incoherent precipitates and fine grains":1st paragraph)**

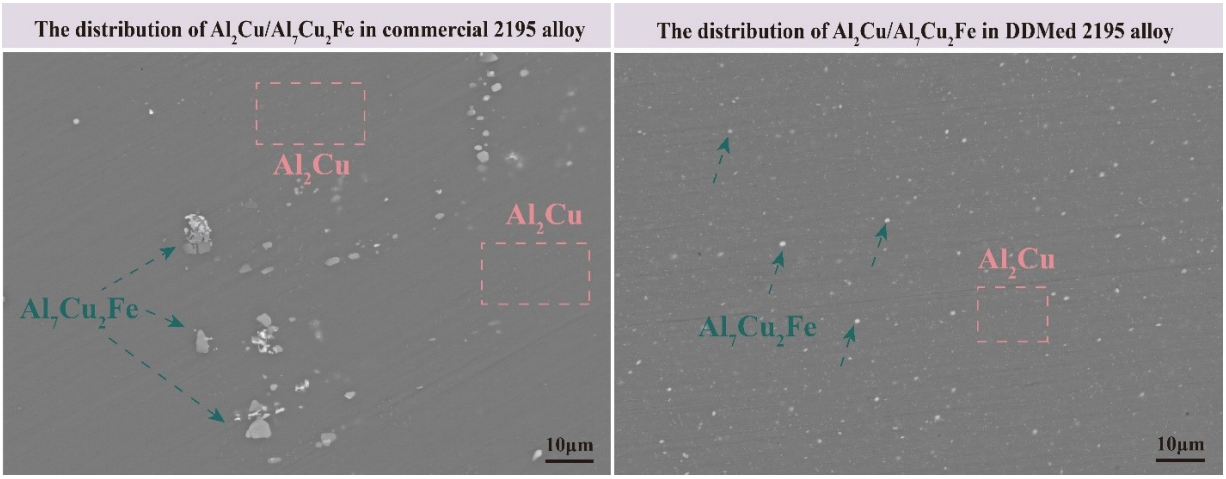

Fig. S1. The distribution of Al_2Cu/Al_7Cu_2Fe in commercial 2195 alloy and DDMed 2195 alloy via scanning electron microscope.

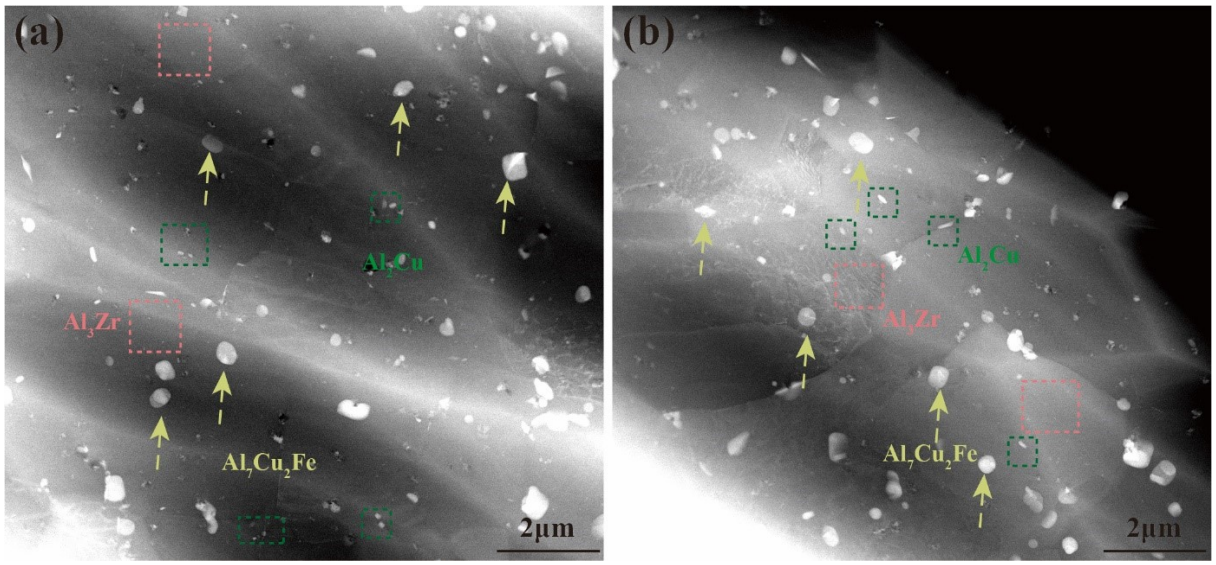

Fig. S2. The distribution of Al_2Cu/Al_7Cu_2Fe in commercial 2195 alloy and DDMed 2195 alloy via scanning transmission electron microscopy.

- **Fig. S3:The grain boundary and the taylor factor of the commercial 2195 alloy /DDMed 2195 (Discussed in "2.2 Coherent-incoherent precipitates and fine grains":6th paragraph)**

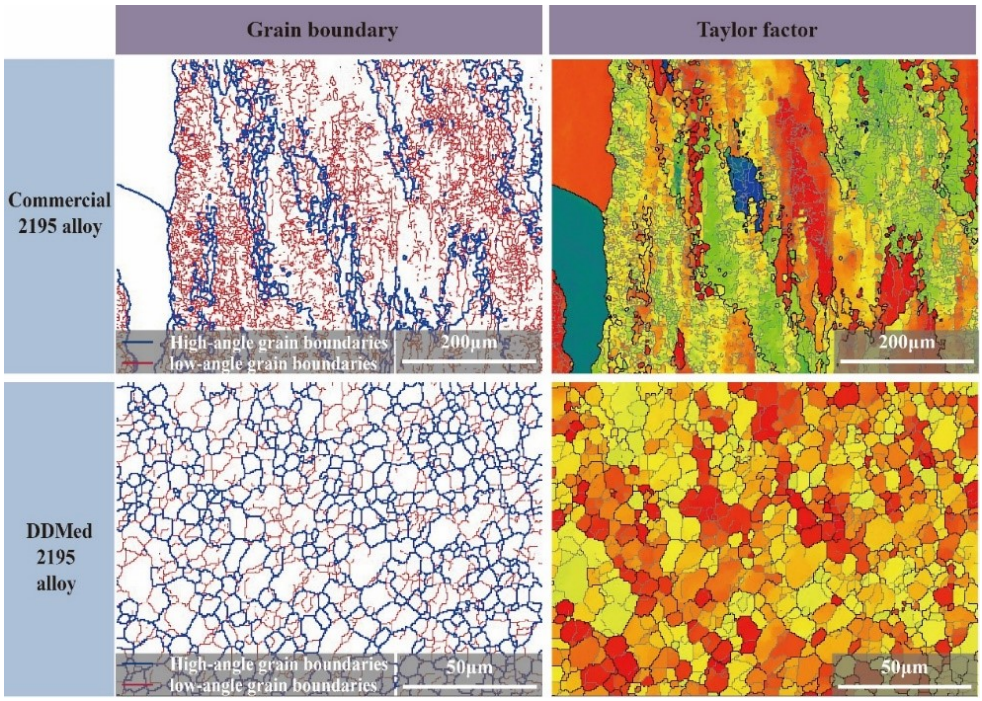

Fig. S3. The grain boundary and the taylor factor of the commercial 2195 alloy/DDMed 2195.

- **Fig. S4:The point-to-point/origin misorientation profile of typical grains in the DDMed 2195 alloy (Discussed in "2.2 Coherent-incoherent precipitates and fine grains":6th paragraph)**

The point-to-origin misorientation varies between approximately 0.0◦ and 1.0◦ and did not accumulate across the grain. Typical multi-peak distributions (Fig.S4b and S4c) within small grains were presented, which were attributed to the intragranular-distributed substructure. Such a phenomenon further clarified the typical characteristics of the DDM method with a high instantaneous plastic strain rate and its dominant continuous dynamic recrystallization mode.

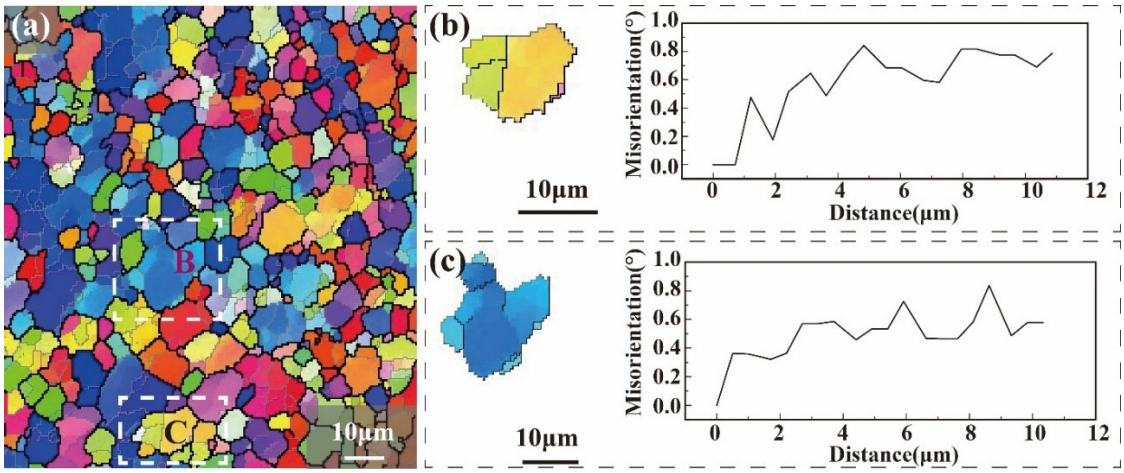

Fig. S4. The point-to-point/origin misorientation profile of typical grains in the DDMed 2195 alloy.

- **Fig. S5: Designed experiments: Let Al-Cu sheets with and without Li undergo friction stir processing at the same time to see the microstructure change. (Discussed in "3.1 Microstructural evolution":3rd paragraph)**

The 2219 sheet (Al-Cu) and the 2195 sheet (Al-Cu-Li) were placed together tightly. The two sheets were undergone friction stir processing at the same time. The phases in the 2219 sheet were the usually-seen coarse θ (Al-Cu) phases. In the 2195 plate, before the severe plastic deformation, the T_1 (Al-Cu-Li) phases were existed, shown in XRD (Fig. S3 E). After the severe plastic deformation, usually-seen needle-like T_1 (Al-Cu-Li) phases were missing instead **by the wave-like stripes with pairs of symmetrical satellite diffraction spot patterns and LPSO (Long Period Stacking Ordered) phases.**

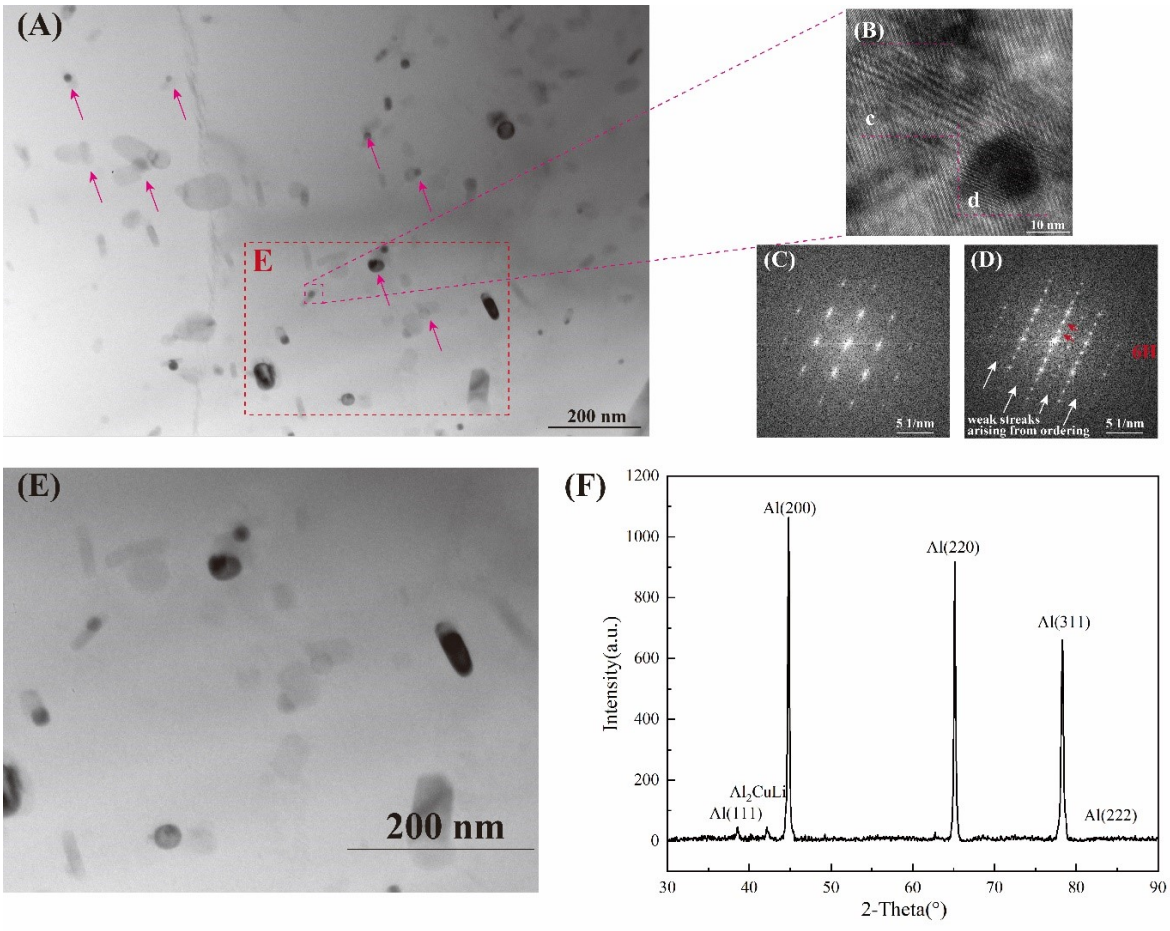

Fig. S5 TEM figure of the 2195 sheet. (A) Bright filed figure of the 2195 sheet. (B) The HR-TEM of the selected phase. (C) The selected area electron diffraction spot patterns of area c. (D) The selected area electron diffraction spot patterns of area d. (E) Magnified view of area E in Figure A (F) The XRD data of the 2195 sheet before the svere plastic deformation.

- **Fig. S6: Bright and dark field figures of the precipitates in the DDMed 2195 alloy (Discussed in "3.1 Microstructural evolution":3rd paragraph)**

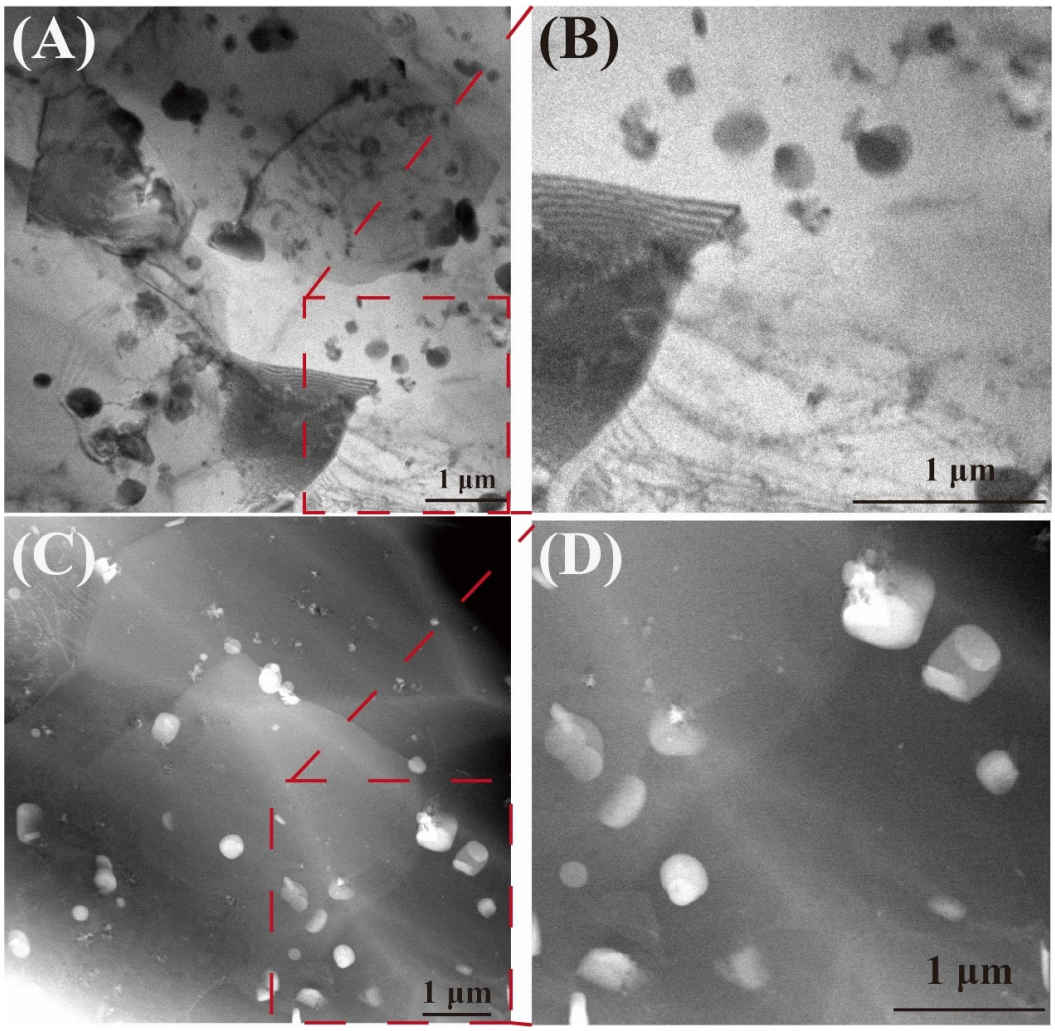

Fig. S6 Bright and dark field figures of the precipitates. (A) Bright field figure. (B) The enlarged figure of the red rectangle in Figure A. (C) Dark field figure. (D) The enlarged figure of the red rectangle in Figure C.

- **Fig. S7: Speculation of dislocation and precipitate interactions process (Discussed in "3.2**

Strength-ductility synergy mechanism":3rd paragraph)

The speculation of dislocation and coherent-incoherent precipitates interactions process was given below:

Different from the Orowan mechanism, dislocations would not accumulate locally around the precipitate, causing stress concentration. Conversely, under the effect of the long-range elastic interactions induced by the core-incoherent structure, the dislocations were pre-bended while cutting through the coherent structure. Thus, the dislocations could glide through the precipitate with increasing strain. And then, the bent dislocations would be straightened under the effect of line tension.

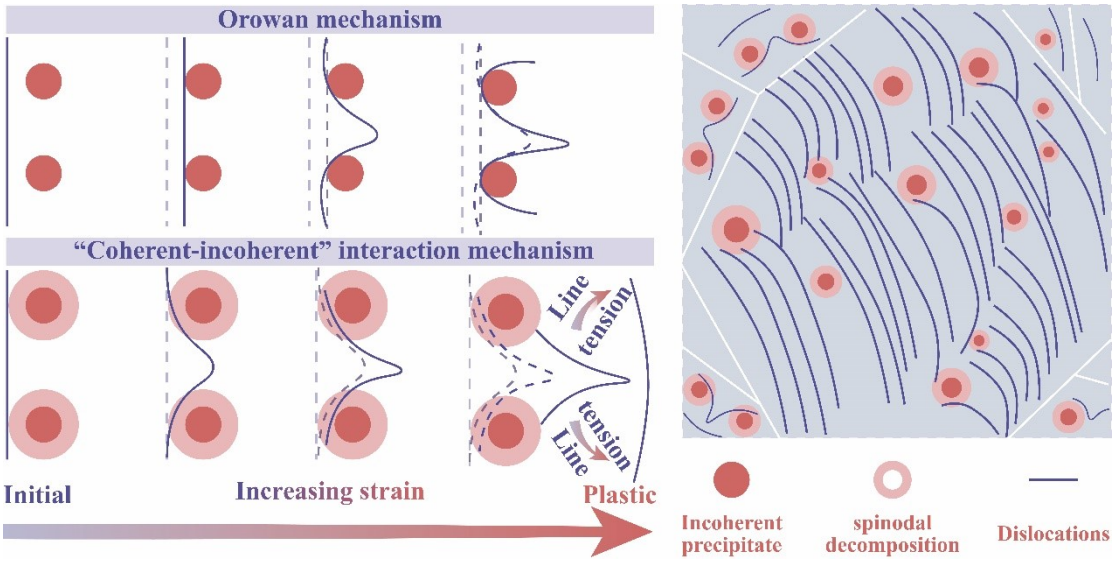

Fig. S7. Schematics of the "coherent-incoherent" strain-hardening mechanisms.

- **Fig. S8: Schematic of the DDM process and the related temperature-time curve (Discussed in "5.1 Materials and preparing process":1st paragraph)**

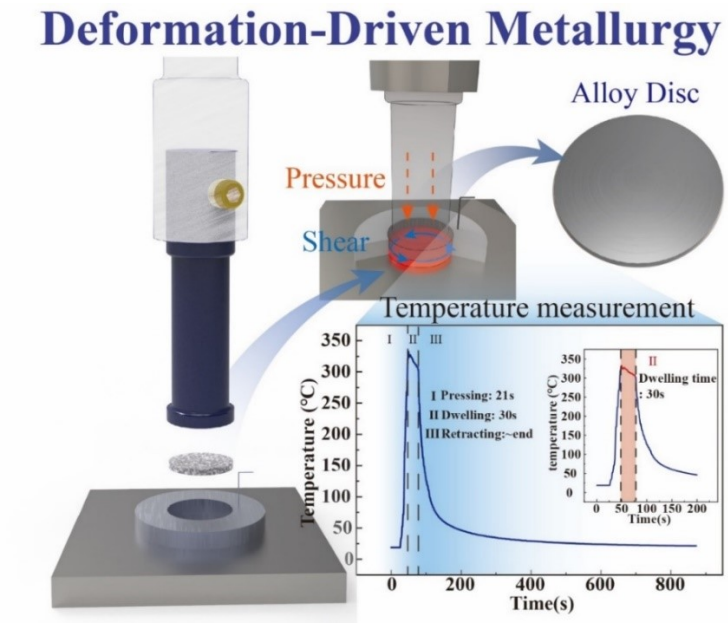

Fig. S8. Schematic of the DDM process and the temperature-time curve during the process.

- **Fig. S9: The selected diffraction spots we used for all GPA analysis (Discussed in "5.2 Characterization":1st paragraph)**

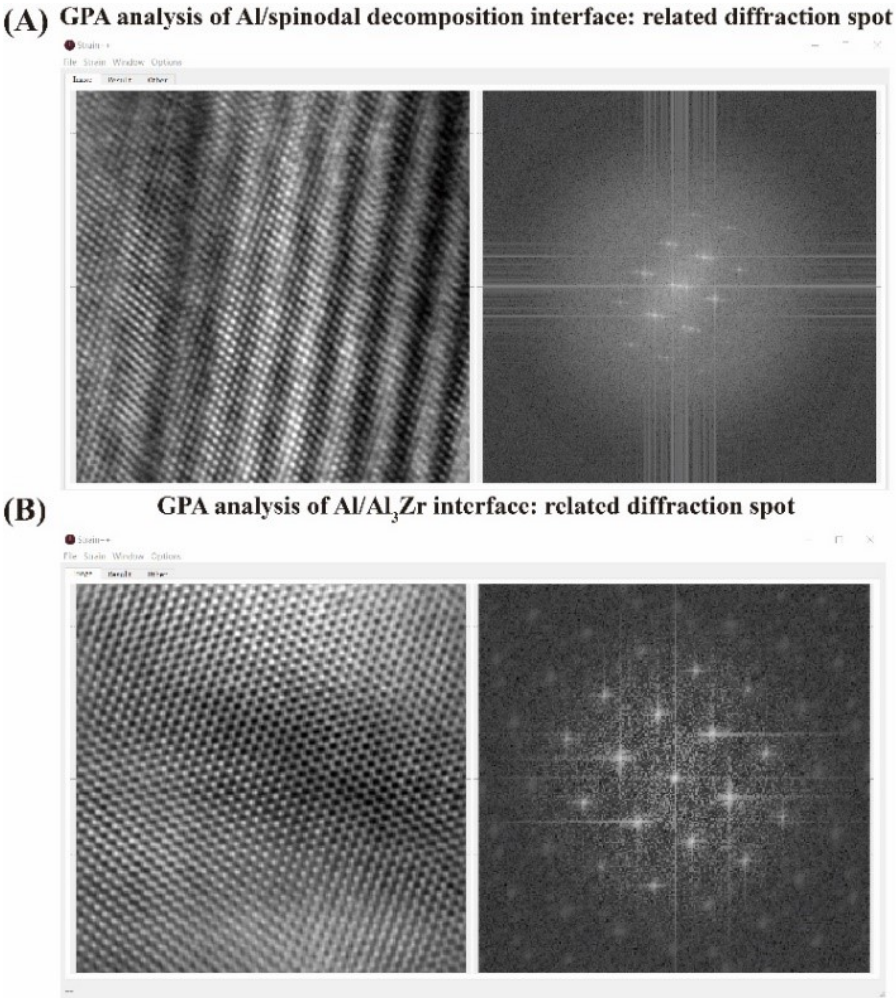

Fig. S9. The selected diffraction spots we used for all GPA analysis.

➢ Videos

Video S1.
The diffraction spots changing at the Al_2Cu/Al interface.

Video S2.
The diffraction spots changing at the Al_7Cu_2Fe/Al interface.